CELLULAR NEUROSCIENCE

Astrocytes and microglia play orchestrated roles and respect phagocytic territories during neuronal corpse removal in vivo

Eyiyemisi C. Damisah[1,2]*, Robert A. Hill[1,3]*, Anupama Rai[1], Fuyi Chen[1], Carla V. Rothlin[4,5], Sourav Ghosh[1,5], Jaime Grutzendler[1,6]†

Cell death is prevalent throughout life; however, the coordinated interactions and roles of phagocytes during corpse removal in the live brain are poorly understood. We developed photochemical and viral methodologies to induce death in single cells and combined this with intravital optical imaging. This approach allowed us to track multicellular phagocytic interactions with precise spatiotemporal resolution. Astrocytes and microglia engaged with dying neurons in an orchestrated and synchronized fashion. Each glial cell played specialized roles: Astrocyte processes rapidly polarized and engulfed numerous small dendritic apoptotic bodies, while microglia migrated and engulfed the soma and apical dendrites. The relative involvement and phagocytic specialization of each glial cell was plastic and controlled by the receptor tyrosine kinase *Mertk*. In aging, there was a marked delay in apoptotic cell removal. Thus, a precisely orchestrated response and cross-talk between glial cells during corpse removal may be critical for maintaining brain homeostasis.

INTRODUCTION

Cell death is an evolutionarily conserved and ubiquitous process occurring in most organ systems throughout life (*1*, *2*) and has been implicated in a variety of homeostatic functions such as developmental tissue patterning, immune regulation, and defense against intracellular infectious pathogens (*3*–*5*). In the central nervous system (CNS), cell death plays an important role in developmental regulation of cell numbers and subtypes in different CNS regions (*3*, *6*) and also in pathological states such as viral infection (*7*).

It is widely recognized that cell death is associated with rapid and robust cellular responses by professional and nonprofessional phagocytes for corpse removal (*8*–*10*). Ineffective clearance of dying cells is implicated in a variety of inflammatory (*11*, *12*), autoimmune (*11*), developmental (*13*), and neurodegenerative conditions (*14*). Because of this, the mechanisms for detection and removal of cells are highly regulated and involve signals derived from dying cells, which activate receptors on phagocytes to initiate corpse engulfment and clearance (*15*).

In the mammalian brain, microglia are regarded as the primary phagocyte responsible for corpse removal; however, under certain conditions, astrocytes have been shown to demonstrate phagocytic capability (*16*, *17*). Mutations in microglia and/or astrocyte genes including *Csf1r* (*18*), *Trem2* (*19*, *20*), and *Mertk* (*21*) have been implicated in neurodegenerative disorders (*15*, *22*, *23*). However, the precise interplay between astrocytes and microglia during corpse removal remains unexplored. Specifically, whether astrocytes and microglia act in concert or independently to remove dying cells or whether each cell population has specialized functions is not known. Furthermore, the molecular mechanisms that mediate the complex dynamic interactions between microglia, astrocytes, and dying cells are not well understood.

Brain phagocytes use a variety of receptors to identify, engage, and engulf cells programmed to die. Among those, the receptor tyrosine kinases *Axl* and *Mertk* are known to mediate the clearance of apoptotic cells by sensing flipped phosphatidylserine on the outer membrane of dying cells, which activates signaling for cytoskeletal rearrangement, leading to phagocytosis (*7*, *24*, *25*). *Axl* and *Mertk* are expressed in both astrocytes and microglia (*26*, *27*); however, the precise function of these receptors has not been fully characterized. Specifically, it is not known how these receptors affect the relative function of astrocytes and microglia or whether they mediate a coordinated interplay between these cells during corpse removal.

Despite the large number of cells that undergo apoptosis daily, visualization of the cell death process, the specific role of phagocytes, and the mechanisms of corpse removal in vivo have been limited. This is partly due to the unpredictable timing and location of apoptosis, the rapid progression of the cell death process, and the efficient removal of apoptotic cells by phagocytes. To address this, we have developed photochemical and viral methodologies to induce death in single cells in the live brain and combined these approaches with intravital optical imaging of the multicellular glial reaction associated with cell death and corpse clearance. This allowed us to track the precise multicellular interactions of defined phagocyte populations during their engagement with a dying cell, with high temporal and spatial resolution in the live brain.

Unexpectedly, we found that astrocytes and microglia acted in a highly coordinated fashion, negotiating the removal of apoptotic cells and debris. Although microglia and astrocytes polarized simultaneously toward the dying cells and displayed a high degree of intermingling during this process, each cell exhibited specialized functions. Astrocytes engulfed diffuse apoptotic bodies derived from the extensive dendritic arbors of dying neurons, by polarizing their distal processes without exhibiting cell body migration. In contrast, microglia predominantly phagocytosed dendrites, cell bodies, and

[1]Department of Neurology, Yale School of Medicine, New Haven, CT, USA. [2]Department of Neurosurgery, Yale School of Medicine, New Haven, CT, USA. [3]Department of Biological Sciences, Dartmouth College, Hanover, NH, USA. [4]Department of Immunobiology, Yale School of Medicine, New Haven, CT, USA. [5]Department of Pharmacology, Yale School of Medicine, New Haven, CT, USA. [6]Department of Neuroscience, Yale School of Medicine, New Haven, CT, USA.
*These authors contributed equally to this work.
†Corresponding author. Email: jaime.grutzendler@yale.edu

nuclei by migrating toward these structures and completely engulfing them. Following reductions in microglia cell density, astrocytes readily compensated by engulfing cell bodies, but the overall process was less efficient. The coordinated responses by microglia and astrocytes were tightly regulated by the receptor tyrosine kinase *Mertk*. This was evidenced by a delayed recognition by microglia and failure of astrocyte polarization toward dying cells in the absence of *Mertk*. Advanced aging was also found to be associated with a delay in the removal of dying neurons.

Overall, our data provide evidence that astrocytes and microglia divide the labor of corpse removal in a highly coordinated fashion. Thus, regulation of microglia-astrocyte orchestration could be critical for recovery of homeostasis in a variety of brain disorders and its defect may contribute to age-related neurodegeneration.

RESULTS

Imaging the coordinated multicellular responses during neuronal corpse clearance in live mice

The efficient and complete removal of dying neurons poses a major challenge to phagocytes given their complex dendritic and axonal arborizations spanning long distances. The extent of involvement of the different brain phagocytes and whether they coordinate their responses during the removal of various parts of a cell in the mammalian brain is not known. In addition, spontaneous cell death in the brain is difficult to capture by live imaging due to its sporadic nature and unpredictable location. To induce apoptosis of individual cells at a desired time and location in the adult mouse brain, we implemented methodologies we recently developed for single cell–targeted ablation using two-photon–mediated photochemically induced apoptosis (2Phatal) (Fig. 1, A and B, and movie S1) (*28*). This method uses a femtosecond-pulsed laser to bleach a nucleic acid binding dye within experimentally targeted cells, which induces a stereotyped apoptotic cell death process without triggering injury-related glial activation (figs. S1 and S2 and movie S2) (*28*). To gain an understanding of the precise dynamics of the different types of glia during corpse removal, we visualized fluorescently labeled glial cells with time-lapse two-photon imaging following 2Phatal-induced apoptotic neuronal death in the live mouse brain.

Multiple glial types compete for cell body engulfment, but a single microglia prevails

We observed that both astrocytes and microglia rapidly and concurrently polarized their processes toward dying cells within 2 to 3 hours after induction of apoptosis (Fig. 1, C, D, F, and G). Although astrocytic and microglial processes were initially heavily intermingled, microglia migrated and fully encapsulated apoptotic cell bodies (Fig. 1C, fig. S3A, and movie S2). In a subset of cases (~20%), we observed no astrocyte polarization after apoptotic induction, which tended to occur when microglia polarized more rapidly toward dying cells. Furthermore, during the microglia polarization process, we observed that multiple microglia in the vicinity of a dying cell projected their processes and started to wrap around the cell; however, within a few hours, the cell body of only one microglia migrated and fully engulfed the dying cell (fig. S3B and movie S3). In addition to the microglia and astrocyte responses, NG2 glia also exhibited a subtle but targeted response to dying cells at 6 hours. In many cases, the polarization of NG2 glia remained at 24 hours despite complete removal of the dead cell and appeared to fill the space left following corpse removal (fig. S4). These data show that following induction of cell death, multiple microglia, astrocytes, and NG2 glia rapidly respond to cues from dying neuronal cell bodies, but eventually only one microglia prevails. This suggests either an intercellular competitive mechanism or precise intercommunication between glial cells to coordinate the engulfment process.

Segregation of function and division of labor between astrocytes and microglia during neurite clearance

Having shown that microglia play a predominant role in the removal of somas, we asked whether the same was true for the removal of dendritic arbors, which might pose a significant challenge given their diffuse nature. We used a combination of microglia reporter mice and sulforhodmaine-101 to label astrocytes and to track these cells in vivo during induction of individual neuronal death. We observed that microglia tended to specialize in engulfing dendritic branches closest to the soma (Fig. 1E and fig. S3, C and D) and tightly wrapped around proximal dendrites with extreme precision (fig. S3, D and E). In contrast to microglia, astrocytes polarized their fine and extensive processes to engulf large numbers of small diffuse apoptotic neuritic fragments, especially those derived from more distal neuronal branches (Fig. 1H and movie S4). This engulfment did not require any mobilization of astrocyte cell bodies, as was seen during microglia engulfment, which may reflect the fact that astrocyte processes are already in close contact with most neuronal branches and may thus be better positioned to compete for phagocytic territory.

Precise phagocytic boundaries between astrocytes and microglia in various models of cell death

To test whether this specialization and functional orchestration between glial cells was present in other modes of cell death, we imaged spontaneously occurring cell death in early postnatal development (Fig. 2, B to D) or after induction of cell death in adults through intracerebral injection of high-titer adeno-associated virus-9 (AAV9) (figs. S5 and S6) (*29*). Using these models and high-resolution fixed tissue confocal imaging, we were able to visualize the cell body and the more distal neurites of dying cells, concurrently with the associated glial reaction. Despite the fact that cell death is a more protracted process in the viral infection model, we found notably similar features, as is seen with apoptotic death during early postnatal development (postnatal day 5) and after 2Phatal. Microglia were found to specialize in engulfing cell bodies and proximal dendrites (Fig. 2, A and B), while astrocytes preferentially engulfed distal processes and diffuse neuritic debris (Fig. 2, A and B, and fig. S7). The processes of microglia and astrocytes were frequently found to be precisely segregated along the surface of dying cell bodies and neurites (Fig. 2, A to D).

Overall, these data reveal that both astrocytes and microglia are concurrently active during corpse removal, but each cell has specific and specialized roles. In addition, a notable feature is that they occupy precise territories and respect each other's boundaries, suggesting the presence of local mechanisms of communication between these cells. This orchestrated response and division of labor may be critical for the effective containment of the disrupted cell bodies and the diffuse processes of apoptotic and virally infected cells.

Mertk is critical for determining the speed of microglia engagement with dying cells

Microglia express a variety of receptors that have been implicated in the recognition and engulfment of dying cells (*30*–*33*). Among those,

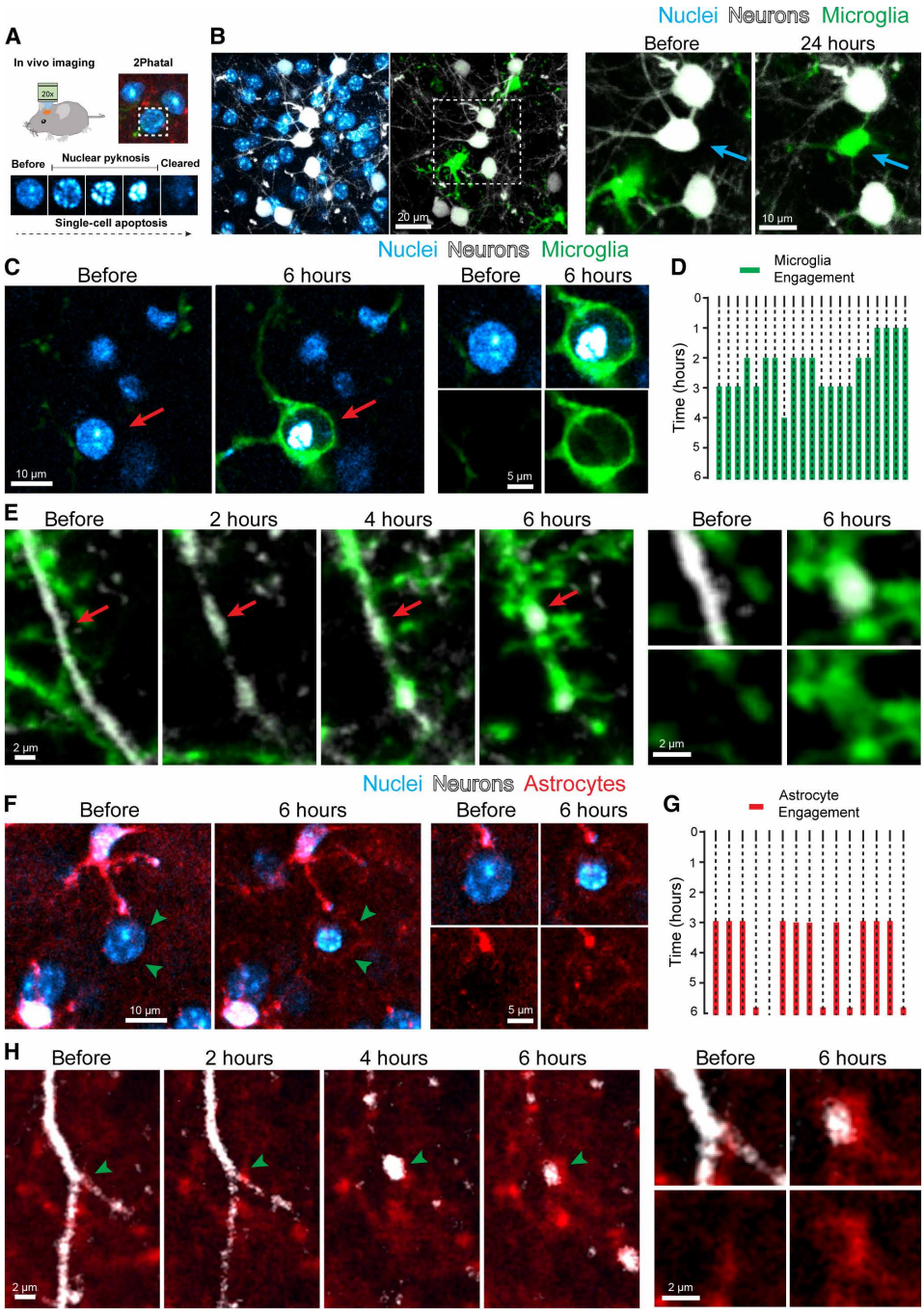

Fig. 1. Live imaging of astrocytes and microglia during cell corpse removal. (**A**) Photochemical ablation and induction of single-cell apoptosis via 2Phatal in live mouse cortex. (**B**) Hoechst 33342 dye labeling of cell nuclei (blue), fluorescently labeled neurons (white), and microglia (green) before 2Phatal. The boxed region is magnified, and time-lapse imaging shows targeting of a single neuron for 2Phatal (blue arrow) followed by a single microglial cell occupying the territory of the ablated neuron 24 hours later. (**C**) Time-lapse imaging showing microglia engulfment of a dying neuron with a condensed nucleus (red arrow). (**D**) Traces depicting 21 cell death events, showing the timing of microglia arrival and engagement with the dying cells from four mice. (**E**) Time-lapse imaging detailing microglia engulfment of apoptotic neurites (red arrows) over 6 hours. (**F**) Time-lapse imaging showing subtle astrocyte polarization around a cell targeted with 2Phatal (green arrowheads). (**G**) Timing of astrocyte engagement with 15 single dying cells collected from four mice. (**H**) Time-lapse imaging showing the dynamic formation of astrocyte polarization around apoptotic neurites over 6 hours (green arrowheads).

the tyrosine kinase receptors *Axl* and *Mertk* have been shown to mediate phagocytosis during developmental and pathological processes (*7*, *24*). *Axl* and *Mertk* are also expressed in astrocytes (*26*, *34*), although their role in these cells is less well understood. To investigate the precise role of *Axl* and *Mertk* during the orchestrated astrocyte-microglia response to dying cells, we implemented our 2Phatal-targeted apoptotic method combined with high-resolution in vivo imaging of glia and neurons in mice lacking either or both receptors.

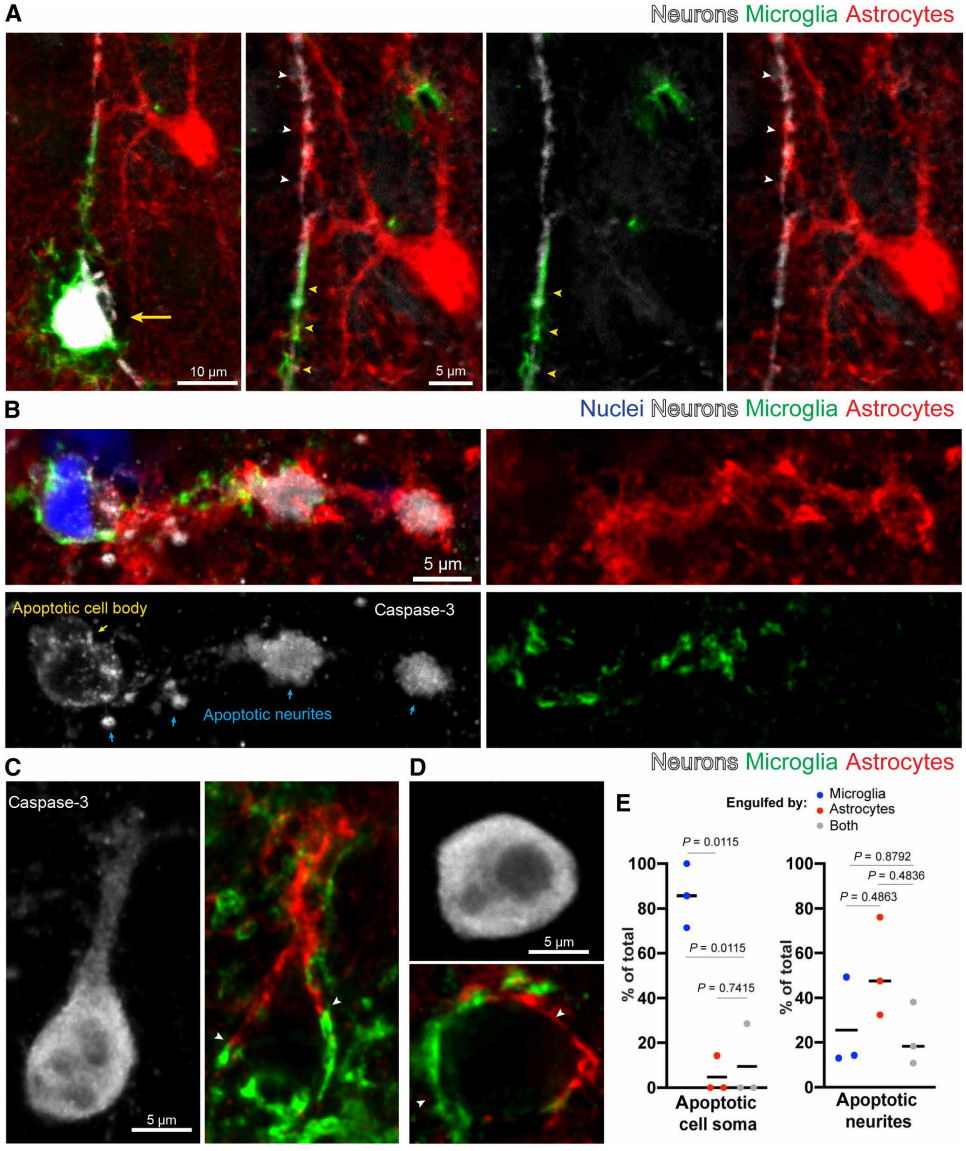

Fig. 2. Territorial segregation of glial processes during cell corpse engulfment. (A) Confocal fluorescence image showing division of labor between microglia (green) and astrocytes (red) during elimination of a neuron (white, yellow arrow) and its apical dendrite, after cell death induction by high-titer adeno-associated virus-9 (AAV9)–green fluorescent protein (GFP) infection. The microglia has converged on the soma and apical dendrite (yellow arrowheads), while the astrocyte surrounds the distal dendrite (white arrowheads), with boundaries observed between processes of these glial cells. (**B**) Confocal fluorescence image of spontaneous cell death during postnatal development in mouse cortex. The soma (yellow arrow) and neurites (blue arrows), labeled via caspase-3, are engulfed by microglia (green), while the distal dendritic processes are engulfed by astrocytes (red). Intermingling of both glia processes is observed in the middle portion of the dendrite. (**C** and **D**) Examples of cells labeled by caspase-3 immunofluorescence showing astrocytes (red) and microglia (green) polarized toward different parts of the dying cell with territorial boundaries (white arrowheads). (**E**) Quantification of the relative engulfment of cell bodies and dendrites by astrocytes and/or microglia following cell death by high-titer AAV9-GFP infection ($n = 3$ mice per group, greater than 50 apoptotic neurites and 20 cell bodies per mouse). Statistics with two-way analysis of variance (ANOVA) with Holm Sidak's multiple comparisons test.

We found that in mice with deletion of *Mertk* (*Mertk*$^{-/-}$), there was a significant delay in the timing of cell body clearance (Fig. 3, A to C). In contrast, *Axl* deletion had no effect on the timing of corpse removal (Fig. 3, A to C). Furthermore, mice with deletion of both *Axl and Mertk* showed no additional delay compared to *Mertk* deletion alone (Fig. 3, A to C). Our ability to image apoptotic events concurrently with the reaction of microglia at high spatiotemporal resolution afforded us the opportunity to precisely discern the specific role of *Mertk* at various stages of apoptotic cell removal. We observed that in *Mertk*$^{-/-}$ mice, there was a delay in the timing of initial microglia process engagement with the dying cells (Fig. 3D) rather than in the overall duration of the phagocytic event (Fig. 3, D to F). These data provide direct in vivo evidence that *Mertk* is critical for determining the speed of engagement of microglia toward dying cells, and its absence provides other glial cells the opportunity to compete for phagocytic territory.

Astrocyte polarization and lysosome recruitment toward dying cells is dependent on the speed of microglia engagement

We had initially observed that astrocytes react quickly by subtle polarization of their fine processes toward dying neurons (Fig. 1F). In

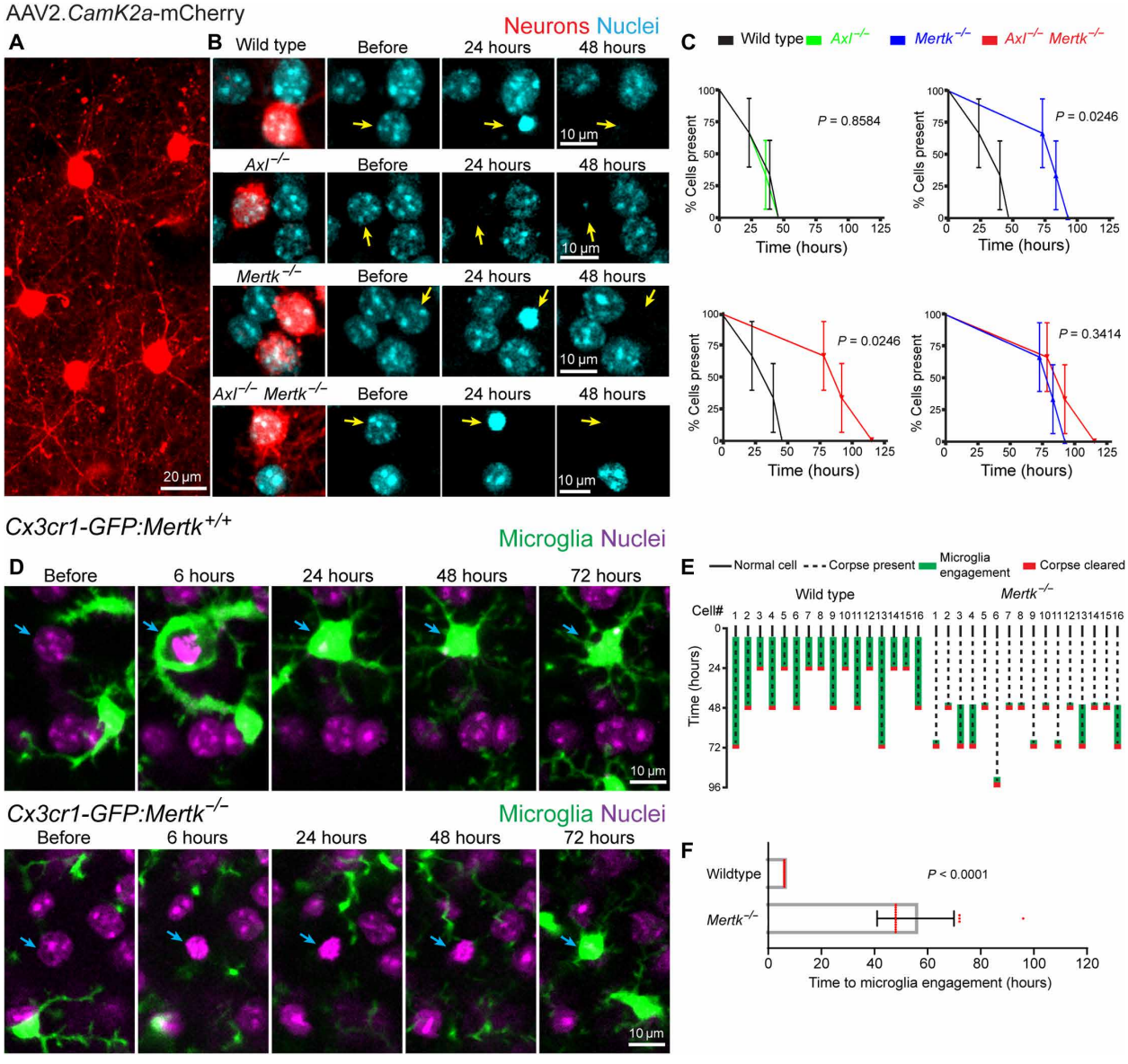

Fig. 3. Deletion of *Mertk*, but not *Axl*, leads to a delay in microglial detection and clearance of apoptotic cells. (**A** and **B**) AAV neuronal labeling and time-lapse imaging detailing the timing of corpse removal after 2Phatal in wild-type, *Axl*$^{-/-}$, *Mertk*$^{-/-}$, and *Axl*$^{-/-}$*Mertk*$^{-/-}$ single- or double-knockout mice. Neuronal corpses were cleared within 24 to 48 hours after 2Phatal in wild-type and *Axl*$^{-/-}$, but remained longer in *Mertk*$^{-/-}$ and *Axl*$^{-/-}$*Mertk*$^{-/-}$ mice. (**C**) Quantification detailing the time to corpse removal after 2Phatal, revealing clearance defects in *Mertk*$^{-/-}$ and *Axl*$^{-/-}$*Mertk*$^{-/-}$ mice but not in *Axl*$^{-/-}$, and no significant additive effects of the double knockout [time to cell clearance: wild type = 41 hours; *Axl*$^{-/-}$ = 37 hours; *Mertk*$^{-/-}$ = 86 hours; *Axl*$^{-/-}$*Mertk*$^{-/-}$ = 96 hours; *P* values as indicated for each comparison, log-rank (Mantel-Cox) test, *n* = 3 mice per group]. (**D**) Visualization of microglia in wild-type and *Mertk*$^{-/-}$ mice revealed that the delayed corpse removal in *Mertk*$^{-/-}$ was caused by delayed microglia engagement with the dying cell. (**E**) Traces depicting 16 wild-type and *Mertk*$^{-/-}$ cells, indicating the timing of cell condensation, microglia engagement, and corpse clearance. (**F**) Average time for initial microglia engagement comparing wild-type and *Mertk*$^{-/-}$ cells (time to engagement: wild type = 6 hours, *Mertk*$^{-/-}$ = 55 hours; $P < 0.0001$, unpaired *t* test, *n* = 16 cells per group).

the subset of cases when there was a very rapid microglia polarization toward the apoptotic cell body, we observed limited concurrent astrocyte polarization. Thus, the speed of microglia engagement with the soma appears to be critical for determining the degree of astrocyte response.

To better understand this process, we used a fluorescent reporter of lysosomes, Lysosomal Associated Membrane Protein 1 [LAMP1–green fluorescent protein (GFP)] in astrocytes to evaluate the phagocytic potential of the astrocyte polarization. Under normal conditions, we observed that in most cases, astrocyte lysosomes were not recruited toward processes contacting dying cells (Fig. 4, A, B, and F). Likewise, deletion of *Mertk* in both astrocytes and microglia resulted in no lysosomal polarization by astrocytes (Fig. 4, D and F). However, when *Mertk* was specifically deleted in microglia (*Csf1r*-cre: *Mertk*$^{fl/fl}$), we found that astrocytes exhibited a robust lysosome polarization toward dying cells (Fig. 4, E and F). Because *Mertk* loss in microglia results in their delayed engagement, these experiments suggest that the timing of microglia engagement is a critical determinant of astrocyte lysosome

polarization. They also suggest that the relative expression and magnitude of *Mertk* signaling in both microglia and astrocytes may determine their speed and degree of coordinated engagement. However, when comparing the timing of corpse removal between global *Mertk*$^{-/-}$ and microglial-specific *Mertk* deletion (*Csf1r-cre/Mertk*$^{fl/fl}$), we found no statistically significant difference (corpses remaining at 48 hours: 100% in *Mertk*$^{-/-}$ and 86% in *Csf1r*-cre: *Mertk*$^{fl/fl}$; $n = 3$ mice per group and 15 cells per genotype; $P = 0.34$). We thus conclude that in the absence of microglia *Mertk*, astrocytes may play a role in the phagocytosis of the dying soma; however, their contribution does not change the overall timing of corpse removal. Therefore, in this situation, the relative contribution of each phagocyte to corpse removal remains to be determined.

A multicellular astrocytic reaction is responsible for cell body removal in the absence of microglia

We have shown that under normal circumstances, astrocytes phagocytose diffuse neurites, but do not phagocytose cell bodies. To determine whether under pathological conditions, astrocytes are capable of compensatory plasticity for cell body removal, we eliminated microglia by administration of the CSF1R antagonist pexidartinib (PLX3397) (fig. S8, A to C) (*35*) while implementing single-cell 2Phatal induction of neuronal apoptosis. We observed a marked delay in the speed of apoptotic cell body removal, as evidenced by the rates of cytoplasm shrinkage and disappearance of labeled nuclei (90% nuclei removal rate at 24 hours in control versus 0% at 24 hours in PLX3397-treated mice; Fig. 5, A to C). We observed that multiple adjacent astrocytes polarized their processes to form a multicellular tight envelope around dying cells, without any migration of their cell bodies (Fig. 5, D and E). In contrast to the transient astrocyte polarization seen in the presence of microglia (Fig. 1F), this astrocytic response persisted and was characterized by a marked polarization of lysosomes at the contact points with the dying cells (Figs. 4C and 5F). As the dying cell cytoplasm gradually shrunk, there was a concurrent tightening of the astrocytic envelopment. Given the absence of other phagocytes in the area and the strong astrocytic lysosome polarization, we speculate that astrocytes engage in gradual digestion in a "piecemeal" fashion rather than full engulfment, which may be mechanistically related to the phenomenon of trogocytosis (*36*). Together, these data show marked astrocytic functional plasticity in the absence of microglia; however, the overall timing of cell body removal is significantly delayed, which may have pathological consequences.

Inefficient corpse clearance in advanced aging

Advanced brain aging is associated with ongoing death in many cell populations (*37*, *38*). Therefore, effective corpse removal is essential to maintain homeostasis. To better understand the effect of glial aging on the kinetics of apoptotic cell removal, we implemented 2Phatal to induce cell death in 26- to 28-month-old mice. We observed that the timing of nuclear condensation following 2Phatal was not significantly different in aged mice compared to 2- to 4-month-old adults (condensed nuclei: 38 of 39 cells at 6 hours in aged mice compared to 48 of 50 cells in adult mice), suggesting that the cell death process was not altered by aging. However, there was a marked delay in the removal of apoptotic nuclei as assessed by in vivo imaging (Fig. 6).

We then aimed to investigate the effects of aging on the glial reaction but had to do this in fixed tissues given the difficulty of breeding aged reporter mice for in vivo imaging. We searched extensively in immunostained tissues to find occasional caspase-3–positive cells with condensed nuclei. In those cases, we observed typical microglia and astrocyte polarization toward spontaneously dying cells (fig. S9); however, in fixed tissues, we were unable to analyze the temporal dynamics of this process. Nevertheless, given the delayed removal of nuclei that we observed in vivo, we conclude that microglia and astrocytes may be impaired in their ability to either sense the apoptotic cell or initiate the phagocytic event or are defective in their digestive capacity following engulfment. The precise molecular mechanisms of these defects are unclear; however, we do not think that this delay is due to *Mertk* deficiency. This idea is supported by recent single-cell transcriptome analysis, showing that *Mertk* levels are similar between adults and aged mice (*39*), and our own quantitative immunofluorescence analysis showing no aging-related reductions in MERTK protein (fig. S10). Further investigation will be required to determine whether the overall delay in corpse removal is due to defects of microglia sensing and engagement with dying cells, coordinated responses with astrocytes, or digestion of engulfed material.

DISCUSSION

Microglia are considered the primary brain resident phagocytes, although astrocytes have also been shown to exhibit phagocytic functions in vitro, during development, and after injury (*16*, *34*, *40*–*43*). It is not known how these cells coordinate their functions and whether they have specialized roles during corpse removal in homeostatic and pathological conditions. Directly answering these questions requires novel techniques for imaging of cell death events concurrently with the multicellular glial reactions at high spatiotemporal resolution in vivo. We have developed methodologies for single cell–targeted photochemical apoptosis (2Phatal) and combined them with dynamic in vivo imaging of astrocytes and microglia. This approach has allowed us to discover the precise and coordinated roles that microglia and astrocytes play in the removal of dying cells in the live intact mammalian brain.

We found that multiple microglia, astrocytes, and NG2 glia in the vicinity of a dying neuron rapidly polarize their processes toward the cell corpse; however, only one microglia migrates to fully engulf the dying cell and proximal dendrites (Fig. 1F and figs. S3 and S4). The role of this initial astrocytic and NG2 glial process polarization is unclear, but it may be aimed at forming an early cellular barrier to prevent dispersion of small apoptotic debris with toxic or infectious materials and limit detrimental immune activation (*44*). We also observed that astrocytes played a predominant role over microglia in the engulfment of the extensive and diffuse processes of dying neurons without cell body migration. One possibility is that astrocytes have extensive arborizations that are in close proximity to most cells and neurites, while microglia are sparsely tiled and require constant movement of their processes to detect and engage dying cells (*45*, *46*). For microglia to engulf an entire cell would require recruitment and polarization of a large number of cells, which would be inefficient, energetically unfavorable, and potentially detrimental. Therefore, astrocytes are better positioned to engulf diffuse apoptotic debris without large-scale migration. Alternatively, there could be unique "eat me" signals in different parts of dying cells (cell body versus dendrites) that may explain the differential responses of astrocytes and microglia (*16*, *17*, *34*, *47*).

Brain phagocytes use a variety of receptors for the removal of corpses from the brain, including *Axl* and *Mertk* (*12*, *17*, *24*, *34*).

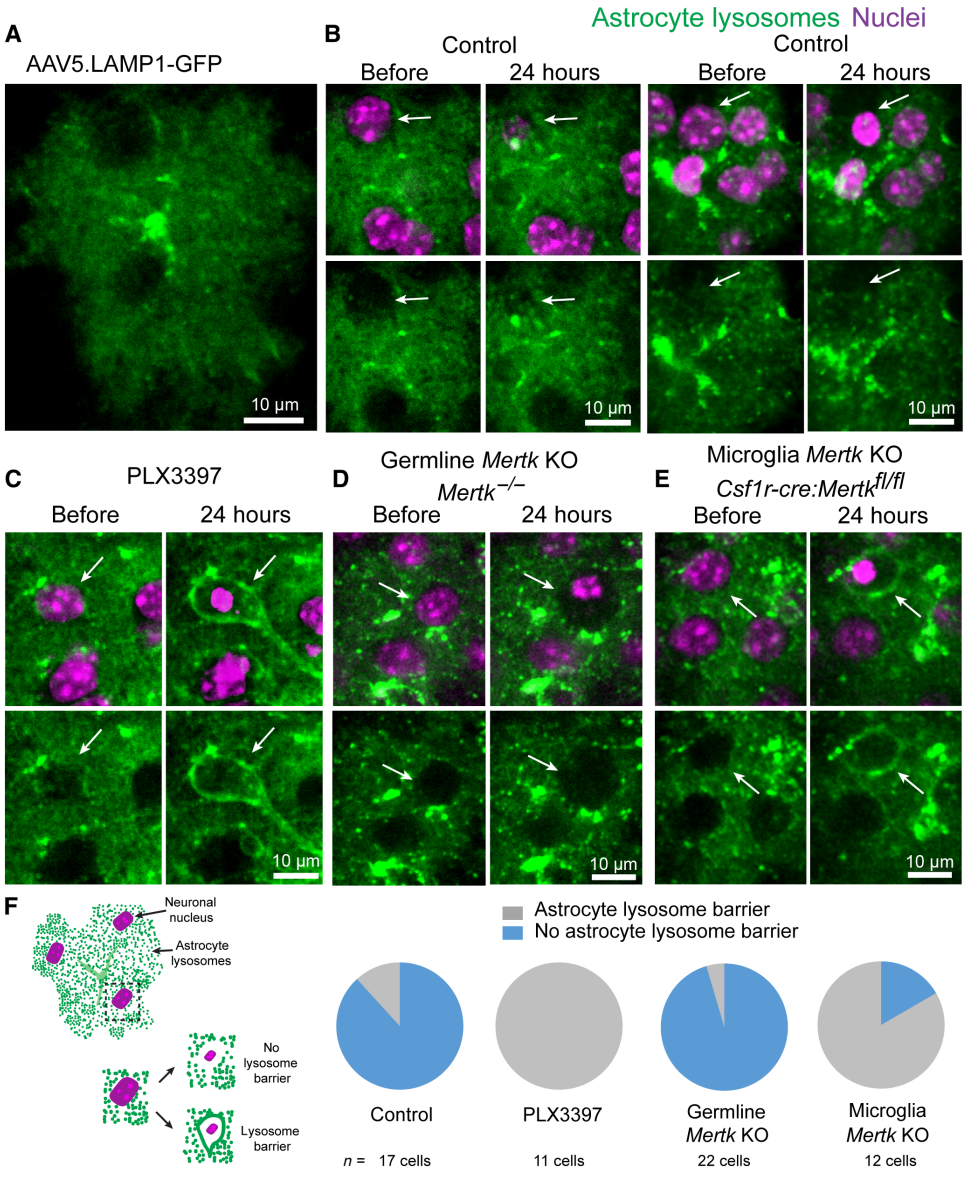

Fig. 4. *Mertk* knockout disrupts astrocyte lysosome polarization toward dying cells. (**A**) Labeling of astrocyte lysosomes after injection of AAV5.LAMP1-GFP into the subarachnoid space in the adult mouse cortex. (**B**) Astrocyte response to dying cells in the presence of microglia in adult wild-type mice. Under normal conditions, astrocyte lysosomes exhibited little to no polarization around the dying cell with condensed nuclei (white arrow). (**C**) After PLX3397-mediated microglia ablation, astrocyte processes polarized lysosomes to gradually digest dying cells (white arrows). (**D**) Astrocytes failed to polarize lysosomes around dying cells in *Mertk*$^{-/-}$ mice. KO, knockout. (**E**) When *Mertk* is deleted exclusively from microglia (*Csf1r*-cre:*Mertk*$^{fl/fl}$), astrocytes polarized lysosomes around the cell corpses, consistent with their response when microglia were completely absent. (**F**) Graphical representation and quantification of lysosome-filled thick astrocyte processes polarized around cell corpses in all groups (control, PLX3397-treated, germline *Mertk* deletion, and microglia-specific *Mertk* deletion, $n = 3$ mice per group).

However, the role of these receptors in the coordinated response of microglia and astrocytes in real time has not been explored. Our intravital imaging and targeted apoptotic approach allowed us to distinguish different aspects of the engulfment process (i.e., time to recognition of dying cells versus overall corpse clearance). We found that disruption of *Mertk* signaling led to a marked delay in the recognition of dying cells by microglia and a failure of astrocytes to polarize and recruit lysosomes (Figs. 3D and 4D). In contrast, *Axl* did not play a significant role in the removal of apoptotic cells in the cortex. This contrasts with observations in the neurogenic region of the subventricular zone, where *Axl* has been found to play a synergistic role with *Mertk* in cell removal (*24*). Deletion of *Mertk* only in microglia or microglia cell depletion elicited a robust compensation by astrocytes, as evidenced by their lysosomal polarization toward the dying cells (Fig. 4, C and E). This suggests that *Mertk* could be an important regulator of the timing of phagocyte engagement and that it may also play a role in astrocyte and microglia cross-talk during corpse removal.

The spatiotemporal orchestration of the astrocyte-microglia reaction not only was an exclusive feature of apoptosis but also was

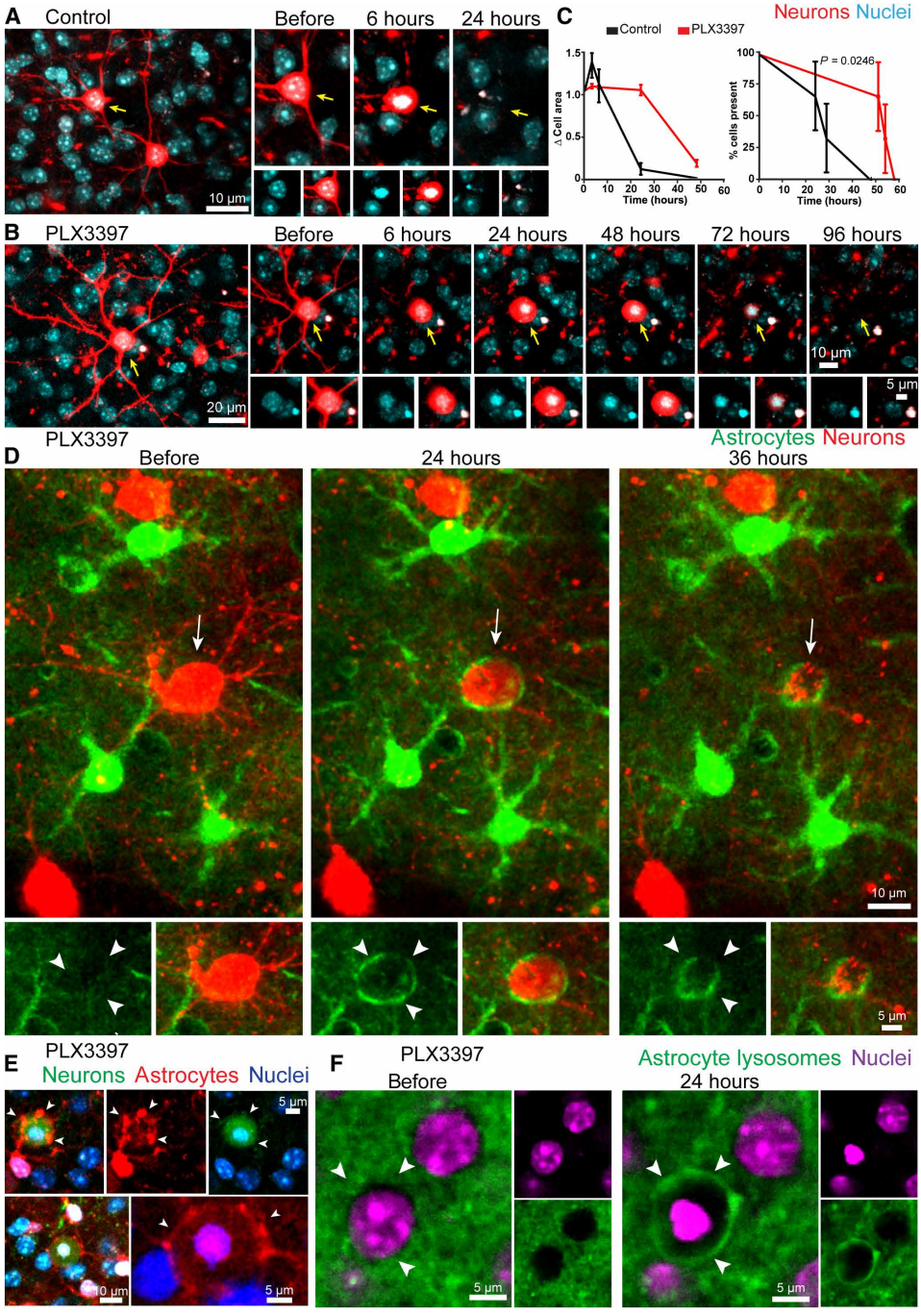

Fig. 5. A multicellular astrocytic reaction mediates phagocytosis after microglia elimination. (**A**) Time-lapse imaging of virally labeled neuron after 2Phatal induction (yellow arrow), showing cell death and corpse clearance occurring over 24 hours. (**B**) Time-lapse imaging of a neuron (yellow arrow) after induction of apoptosis in a PLX3397-treated mouse. In the absence of microglia, the cytoplasm of the apoptotic neuron remained stable for an additional 24 to 48 hours, with corpse removal occurring 48 to 78 hours after 2Phatal induction. (**C**) The relative change in cell body size and timing of apoptotic cell clearance in control- and PLX3397-treated cohorts [time to cell clearance: control = 28.9 hours; PLX3397 = 55.1 hours; $P = 0.0246$, log-rank (Mantel-Cox) test, 15 single cells per mouse, $n = 3$ mice per group]. (**D** and **E**) Delayed corpse removal in the absence of microglia resulted in astrocyte polarization around the dying cell (white arrows and arrowheads). Neuron and astrocyte labeled via AAV infection or with SR101 fluorescent dye for astrocytes (red) in a Thy1-YFP mouse neuron labeling (green). In the absence of microglia, astrocytes did not move their cell bodies during the formation of the barrier. (**F**) AAV labeling of lysosomes reveals astrocytic lysosome polarization (arrowheads) around a cell corpse in a PLX3397-treated animal.

observed in a viral AAV9 infection model and spontaneously occurring cell death. Regardless of the mode of death, astrocytes and microglia engaged dying cells in a coordinated and stereotypical fashion whereby they precisely respected each other's phagocytic territories. One possible explanation could be that phagocyte processes in the vicinity of dying cells detect eat me signals and polarize their processes, restricting access of these signals to neighboring phagocytes, thereby suggesting a competitive process between glial

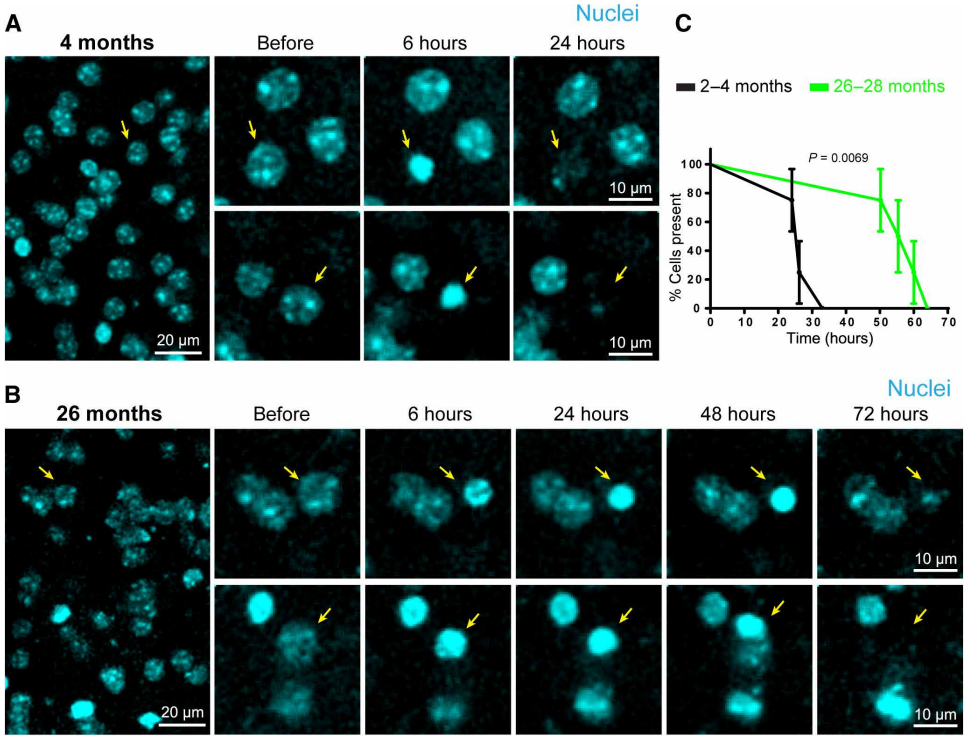

Fig. 6. Aging disrupts the timing of cell corpse removal. (**A**) Time-lapse images detailing: before, 6 hours after, and 24 hours after 2Phatal induction of apoptotic cell death in a 4-month-old mouse. Cells targeted for ablation labeled via Hoechst dye (cyan with yellow arrows). (**B**) Time-lapse images detailing: before, 6 hours after, 24 hours after, and up to 72 hours after 2Phatal induction of 2Phatal apoptotic cell death in a 26-month-old mouse. Cells targeted for ablation labeled via Hoechst dye (cyan with yellow arrows). (**C**) Significant difference in the time course of apoptotic cell removal in 4-month-old versus 26-month-old mice [time to clearance: 4 months = 26.2 hours; 26 months = 57.7 hours, $P = 0.0069$, $n = 4$ mice per group, log-rank (Mantel-Cox) test].

cells. There could also be specialized and dynamic signals (*48*) for lateral inhibition leading to territorial segregation between astrocytes and microglia, which are yet to be discovered.

Together, our data have uncovered a previously unappreciated orchestrated response of microglia, astrocytes, and NG2 glia during the removal of dying neurons from the brain. Astrocytes and microglia have specialized functions in the removal of either large cell bodies or small diffuse debris and demonstrate remarkable territorial precision during this process. The relative contributions of each cell type can be plastic depending on the timing and availability of each phagocyte and is further regulated by the tyrosine kinase receptor *Mertk*. The predominant microglia specialization in cell body removal could be important for preventing the spread of viral particles that have entered the nucleus or pro-inflammatory double-stranded DNA. On the other hand, astrocytes effectively remove the large volume of diffuse microdebris resulting from the death of single cells, particularly in the case of large neurons. The delay in cell body removal that we observed in aging could be a previously unrecognized mechanism of homeostatic disruption that leads to neurodegeneration, autoimmunity, and differential responses to infectious agents.

MATERIALS AND METHODS

Transgenic mouse strains

All experimental procedures were approved by the Institutional Animal Care and Use Committee at Yale University. Male and female mice aged P5 to P840 housed in a 12-hour light/dark cycle with three to five animals per cage were used in these studies. The following transgenic lines were used for visualization of various cell populations in the live brain: *Cx3cr1*$^{GFP/+}$ (Jax #005582); *Thy1*-YFP-H (Jax #003782); *Aldh1l1cre/ERT2* (Jax #029655); NG2cre (Jax #008533); Z/EG (Jax #003920); tdTomato Ai9 (Jax # 007909); *Axl*$^{-/-}$, *Mertk*$^{-/-}$, and *Axl*$^{-/-}$/*Mertk*$^{-/-}$ (*49*); and Csf1^{cre}*Mertk*$^{fl/fl}$ (*24*). Daily intraperitoneal injections of tamoxifen (75 mg/kg for 4 days total) as a solution in corn oil (Sigma) were given to induce Cre recombination and initiate fluorescent reporter expression. Adult *Cx3cr1*$^{GFP/+}$ mice were used for all experiments involving microglia imaging. A sample size of at least three mice (of either sex) was randomly allocated to experimental groups.

Antibodies and reagents

Anti-Iba1 polyclonal antibody (Wako, 019-19741) was used to label microglia. Anti-Aldh1L1 polyclonal antibody (NeuroMab, P28037), anti-GFAP (glial fibrillary acidic protein) (Dako, Z0334), and rabbit anti-S100ß (DAKO GA504) antibodies were used for astrocyte labeling. Anti-MERTK antibody (R&D Systems, AF591) was used for MER proto-oncogene tyrosine kinase (MERTK) labeling. Anti-cleaved caspase-3 rabbit antibody (D175; Cell Signaling Technology) was used for apoptotic cell labeling. Hoechst 33342 (H3570, Thermo Fisher Scientific) was used to label DNA and cell nuclei. Anti-MLKL, clone 3H1 (MABC604), was used for necroptotic cell labeling. Secondary antibodies for immunohistochemistry were fluorophore-conjugated anti-goat (A-21447, Thermo Fisher Scientific), anti-rabbit (A-31572,

Thermo Fisher Scientific), and anti-mouse (A-21202, Thermo Fisher Scientific). Pexidartinib (PLX3397) was purchased from MedKoo Inc. (#206178) and used for pharmacological ablation of microglia. Texas Red dextran (molecular weight, 70,000; Life Technologies, catalog number D-1864) was used for cerebral vessel labeling in vivo.

AAV constructs and production

Virus construct production was done as previously described (*50*). Briefly, the DNA sequence of lysosome-tagged GFP was ligated between the inverted terminal repeat sites of an AAV packaging plasmid with CAG promoter and WPRE/SV40 sequence. Human embryonic kidney (HEK) 293T cells were cotransfected with this construct and a helper plasmid pDP2 (PlasmidFactory, #PF402) for 96 hours and harvested. Virus was purified through iodixanol density centrifugation and titrated by infecting HEK293T cells. Additional viral vectors were purchased as follows: pENN.AAV9.CB7.CI.eGFP.WPRE.rGB (Addgene, catalog no. 105542; AAV9 with 1×10^{13} vg/ml) was used for in vivo labeling and cell death induction (high-titer virus) of neurons. rAAV2/CamKIIa-mCherry (UNC Gene Therapy Vector Core) was used for in vivo neuron labeling. AAV5-GFA104-eGFP.WPRE.bGH (Penn Vector Core, #AAV-5-PV2380) was used to label astrocytes in vivo.

AAV injections

CamKIIa-mCherry and AAV5.*GFAP*-GFP or AAV9.CB7.CI.eGFP was injected into mouse subarachnoid space, as previously described (*50*). Briefly, mice were anesthetized using ketamine-xylazine. A thin skull window about 1 mm in diameter was made with a high-speed drill at 6 mm anteroposterior, 3 mm mediolateral from bregma. The tip of a 30-gauge needle was used to lift about 300 μm by 300 μm piece of thinned skull to expose the underlying dura. The stock solutions of *CamKIIa*-mCherry and AAV5.*GFAP*-GFP were diluted in fresh sterile (1:20, v/v) phosphate-buffered saline (PBS) solution at room temperature before being placed on ice. For AAV9.CB7.CI.eGFP infusion, the stock solution was diluted in fresh sterile (1:10, v/v) PBS solution. The solution was filled into a tygon tube connected to a polypropylene tip with an outer diameter of 70 μm. A programmable syringe pump with a Hamilton syringe was connected to the tube. The tip was then inserted into the subarachnoid space and fixed with cyanoacrylate glue. Diluted *CamKIIa*-mCherry (10 μl) combined with AAV5.*GFAP*-GFP (1:1, v/v) or AAV9.CB7.CI.eGFP solution was injected at speed of 0.2 μl per min. After injection, the tip was removed, and the mouse scalp was sutured. Mice were put on a heating pad for recovery. For stable fluorescent expression, mice were imaged 3 weeks after subarachnoid injection.

Cranial window surgery

The cranial window procedure for topical application of florescent dyes was performed as previously described (*28*). Briefly, animals were anesthetized with intraperitoneal injection of ketamine (100 mg/kg) and xylazine (10 mg/kg). The scalp was shaved and sterilized. A midline incision was performed to expose the underlying skull. A custom-made plate was fixed to the skull with cyanoacrylate glue. An area no larger than 5-mm skull was removed for imaging with dye labeling. Dye was applied to the cortical surface as described below. For fluorescent DNA labeling, Hoechst 33342 (H3570 Thermo Fisher Scientific) was applied directly to the exposed cortex in a 1:250 (v/v; 0.04 mg ml^{-1} diluted in PBS) dilution in PBS from stock solution for 5 min and then washed thoroughly with PBS. After dye labeling, a #0 glass coverslip was cut to size, placed over the craniotomy, and glued in place. After craniotomy, the mice were put on a heating pad for recovery and two-photon imaging was performed 24 hours after dye application.

In vivo two-photon imaging

Mice were anesthetized by either isoflurane or intraperitoneal injection of ketamine and xylazine. Anesthetized mice were head-restrained using a custom-made metal screw and fitted under a two-photon microscope (Prairie Technologies). Images were captured using a mode-locked MaiTai tunable laser (Spectra Physics) with a 20× water immersion objective [1.0 numerical aperture (NA), Zeiss]. The femtosecond laser was tuned to the following wavelengths for two-photon excitation: Hoechst 33342, 775 nm; GFP/YFP (yellow fluorescent protein), 800 to 900 nm; sulforhodamine 101 (SR101), 800 to 900 nm; and *CamKIIa*-mCherry, 775 nm. All images were obtained at depths up to 300 μm from the pial surface. For each cell, *XYZ* stacks were taken from a 209-μm (*X*, 1024 pixels), 209-μm (*Y*, 1024 pixels), and 100-μm (*Z*; step size, 3 μm) volume before any cell manipulation was done. After cell manipulation, the same *XYZ* stack images were taken at identical resolution. For longitudinal imaging, a landmark picture was taken of the pial vessels at the surface of the craniotomy window. All coordinates of imaging regions relative to the landmark vessels were documented. In later imaging sessions, relocation was achieved by matching the blood vessel shape and orientation to the original landmark picture documented.

Induction of apoptotic cell death with 2Phatal

Induction of apoptotic cell death with 2Phatal was done as we previously described (*28*). Briefly, to induce apoptotic cell death via 2Phatal, nuclei were labeled in vivo using Hoechst 33342. Photochemical bleaching of cell nucleus was achieved by focusing a 20- to 40-mW two-photon laser beam for 10 s on a 20 × 20 pixel (8 μm × 8 μm) region of interest (ROI), selected, and centered on the nucleus of a targeted, fluorescently labeled neuron (*28*). Laser wavelength was set to 775 nm, and pixel dwell time was set to 100 μs for all experiments. Images were obtained before 2Phatal and every 2 to 3 hours thereafter until complete phagocytosis of the targeted cell was achieved. The short photo-bleach time and low laser power ensured that there was no laser-induced thermal injury or cell rupture, as we previously described (*28*).

In utero electroporation

PbCAG-TdTomato was used for neuronal labeling via in utero electroporation. In utero electroporation was conducted at embryonic day 17 to label layer II neurons, as previously described (*51*). Briefly, pregnant mice were anaesthetized with a mixture of ketamine (100 mg/kg) and xylazine (10 mg/kg). The abdominal region was shaved and sterilized. A midline incision was made in the skin and abdominal muscles. The uterine horns were exposed, and the lateral ventricle of each embryo was targeted with a glass micropipette and pressure-injected (Picospritzer II, General Valve) with plasmid DNA (~0.5 μl volume per embryo) at a concentration of 1 μg μl^{-1}. This was followed by electroporation with tweezertrodes (50 V, 4- to 50-ms pulses, with 1-s pulse interval; BTX Harvard Apparatus) to target layer II/III cortical neurons. The embryos were placed back in the abdominal cavity, and the muscle and skin were sutured. Electroporated pups were aged to postnatal day 60, and a craniotomy was performed over the transfected hemisphere to carry out the experiments.

Pexidartinib (PLX3397) administration

Pexidartinib (PLX3397) was purchased from MedKoo Inc. (#206178) and used for pharmacological ablation of microglia. PLX3397 was administered orally, as previously described (*35*). Briefly, PLX3397 was formulated in standard chow Teklad diet and provided at 290 mg/kg. Twenty-one days of PLX3397 administration was used for all experiments.

SR101 labeling

SR101 (Sigma-Aldrich, catalog no. S7635) was applied to the cortex to label astrocytes in vivo, as previously described (*52*, *53*). Briefly SR101 was directly applied to the cortical surface for 5 to 10 min at a concentration of 50 μM and then washed thoroughly for 10 min or 100 μl was injected intravenously at a concentration of 5 mM dissolved in PBS.

Immunohistochemistry

Mice were anesthetized and perfused with PBS and 4% paraformaldehyde. Whole-brain tissue was postfixed overnight in 4% paraformaldehyde at 4°C. Brain tissue sections (50 μm thick) were cut on a vibratome and processed for immunohistochemistry. Tissue sections were blocked in 1× PBS containing 5% normal donkey serum and 0.1% Triton X-100 at room temperature. All primary and secondary antibodies were diluted in 1× PBS containing 5% normal donkey serum and 0.1% Triton X-100. Tissue sections were incubated in primary antibodies overnight at 4°C and secondary antibodies for 2 hours at room temperature.

Confocal microscopy

A Leica SP5 confocal microscope with a 20× water immersion objective (1.0 NA, Leica) or a 63× oil immersion objective (1.40 NA, Leica) was used. Applicable laser excitation wavelengths and acousto-optical beam splitter settings were used for optimal fluorophore excitation and emission separation and detection.

Image processing and quantification

Cell body area (Fig. 5) was calculated using a custom-made macro based on National Institutes of Health (NIH) ImageJ/Fiji. The cell body area for each neuron was extracted from the original *XYZ* stack by making a three–optical slice maximal projection centered at the middle plane of the soma. The image stack was then run through a "despeckle" filter to remove noise and thresholded. The same procedure was performed for all time points. Area measures were calculated with Fiji and compared across time points. To quantify mean florescence intensities (figs. S2, S7, and S10), images were acquired using the same microscope settings in all experimental groups. Each cell used for analysis was extracted from the original *XYZ* stack by making a three–optical slice maximal projection centered at the middle plane of the cell. ROIs were selected using the freehand tool. The ROI manager was then used to save the selection in all channels, and a macro on NIH ImageJ was used to measure fluorescence intensity.

Statistical analysis

Statistical differences in astrocyte and/or microglia contribution to cell body or neurite removal, after virus-mediated cell death (Fig. 2), were determined using two-way analysis of variance with Holm Sidak's multiple comparison test. For quantification of apoptotic cell death after 2Phatal (Figs. 1 and 3 to 6), cell nuclei were classified as normal, condensed, or absent based on our previous characterization (*28*) and as indicated in the text and figures. Statistical differences for cell corpse removal (cell survival analysis) following 2Phatal were determined using the log-rank (Mantel-Cox) test for cell survival analysis (Figs. 3, 5, and 6). For quantification of microglia cell densities in *Cx3cr1*-GFP$^{GFP/+}$ control and PLX3397-treated mice (fig. S8), unpaired Student's *t* test was used to determine statistical significance. All data were assumed to have a normal distribution and equal variance for each statistical test and plotted as the mean ± SEM, as indicated in each figure legend. No data were excluded from analysis, no randomization was used to assign experimental subjects, and experimenter blinding was not necessary. No statistical methods were used for predetermined sample size determination. For each experiment, animal and cell numbers are indicated in the text/figure legend. Each representative image was successfully repeated in excess of at least three image locations for each animal with sample sizes (*n*) designated as single cells followed over multiple days or single animals imaged, as indicated in the text and figure legends.

SUPPLEMENTARY MATERIALS

Supplementary material for this article is available at http://advances.sciencemag.org/cgi/content/full/6/26/eaba3239/DC1

View/request a protocol for this paper from *Bio-protocol*.

REFERENCES AND NOTES

1. Y. Fuchs, H. Steller, Programmed cell death in animal development and disease. *Cell* **147**, 742–758 (2011).
2. J. Yuan, B. A. Yankner, Apoptosis in the nervous system. *Nature* **407**, 802–809 (2000).
3. R. E. Ellis, J. Y. Yuan, H. R. Horvitz, Mechanisms and functions of cell death. *Annu. Rev. Cell Biol.* **7**, 663–698 (1991).
4. P. Danthi, Viruses and the diversity of cell death. *Annu. Rev. Virol.* **3**, 533–553 (2016).
5. M. D. Jacobson, M. Weil, M. C. Raff, Programmed cell death in animal development. *Cell* **88**, 347–354 (1997).
6. D. G. Southwell, M. F. Paredes, R. P. Galvao, D. L. Jones, R. C. Froemke, J. Y. Sebe, C. Alfaro-Cervello, Y. Tang, J. M. Garcia-Verdugo, J. L. Rubenstein, S. C. Baraban, A. Alvarez-Buylla, Intrinsically determined cell death of developing cortical interneurons. *Nature* **491**, 109–113 (2012).
7. Y. Tufail, D. Cook, L. Fourgeaud, C. J. Powers, K. Merten, C. L. Clark, E. Hoffman, A. Ngo, K. J. Sekiguchi, C. C. O'Shea, G. Lemke, A. Nimmerjahn, Phosphatidylserine exposure controls viral innate immune responses by microglia. *Neuron* **93**, 574–586.e8 (2017).
8. V. A. Fadok, D. L. Bratton, D. M. Rose, A. Pearson, R. A. B. Ezekewitz, P. M. Henson, A receptor for phosphatidylserine-specific clearance of apoptotic cells. *Nature* **405**, 85–90 (2000).
9. R. Parnaik, M. C. Raff, J. Scholes, Differences between the clearance of apoptotic cells by professional and non-professional phagocytes. *Curr. Biol.* **10**, 857–860 (2000).
10. W. Wood, M. Turmaine, R. Weber, V. Camp, R. A. Maki, S. R. McKercher, P. Martin, Mesenchymal cells engulf and clear apoptotic footplate cells in macrophageless PU.1 null mouse embryos. *Development* **127**, 5245–5252 (2000).
11. S. Nagata, R. Hanayama, K. Kawane, Autoimmunity and the clearance of dead cells. *Cell* **140**, 619–630 (2010).
12. S. Arandjelovic, K. S. Ravichandran, Phagocytosis of apoptotic cells in homeostasis. *Nat. Immunol.* **16**, 907–917 (2015).
13. A. E. Hochreiter-Hufford, C. S. Lee, J. M. Kinchen, J. D. Sokolowski, S. Arandjelovic, J. A. Call, A. L. Klibanov, Z. Yan, J. W. Mandell, K. S. Ravichandran, Phosphatidylserine receptor BAI1 and apoptotic cells as new promoters of myoblast fusion. *Nature* **497**, 263–267 (2013).
14. J. I. Etchegaray, E. J. Elguero, J. A. Tran, V. Sinatra, M. B. Feany, K. McCall, Defective phagocytic corpse processing results in neurodegeneration and can be rescued by TORC1 activation. *J. Neurosci.* **36**, 3170–3183 (2016).
15. M. Prinz, J. Priller, Microglia and brain macrophages in the molecular age: From origin to neuropsychiatric disease. *Nat. Rev. Neurosci.* **15**, 300–312 (2014).
16. Y. M. Morizawa, Y. Hirayama, N. Ohno, S. Shibata, E. Shigetomi, Y. Sui, J. Nabekura, K. Sato, F. Okajima, H. Takebayashi, H. Okano, S. Koizumi, Reactive astrocytes function as phagocytes after brain ischemia via ABCA1-mediated pathway. *Nat. Commun.* **8**, 28 (2017).
17. T. Iram, Z. Ramirez-Ortiz, M. H. Byrne, U. A. Coleman, N. D. Kingery, T. K. Means, D. Frenkel, J. el Khoury, Megf10 is a receptor for C1Q that mediates clearance of apoptotic cells by astrocytes. *J. Neurosci.* **36**, 5185–5192 (2016).

18. R. Rademakers, M. Baker, A. M. Nicholson, N. J. Rutherford, N. Finch, A. Soto-Ortolaza, J. Lash, C. Wider, A. Wojtas, M. DeJesus-Hernandez, J. Adamson, N. Kouri, C. Sundal, E. A. Shuster, J. Aasly, J. MacKenzie, S. Roeber, H. A. Kretzschmar, B. F. Boeve, D. S. Knopman, R. C. Petersen, N. J. Cairns, B. Ghetti, S. Spina, J. Garbern, A. C. Tselis, R. Uitti, P. Das, J. A. van Gerpen, J. F. Meschia, S. Levy, D. F. Broderick, N. Graff-Radford, O. A. Ross, B. B. Miller, R. H. Swerdlow, D. W. Dickson, Z. K. Wszolek, Mutations in the colony stimulating factor 1 receptor (CSF1R) gene cause hereditary diffuse leukoencephalopathy with spheroids. *Nat. Genet.* **44**, 200–205 (2011).
19. R. Guerreiro, A. Wojtas, J. Bras, M. Carrasquillo, E. Rogaeva, E. Majounie, C. Cruchaga, C. Sassi, J. S. K. Kauwe, S. Younkin, L. Hazrati, J. Collinge, J. Pocock, T. Lashley, J. Williams, J.-C. Lambert, P. Amouyel, A. Goate, R. Rademakers, K. Morgan, J. Powell, P. St George-Hyslop, A. Singleton, J. Hardy; Alzheimer Genetic Analysis Group, TREM2 variants in Alzheimer's disease. *N. Engl. J. Med.* **368**, 117–127 (2013).
20. T. Jonsson, H. Stefansson, S. Steinberg, I. Jonsdottir, P. V. Jonsson, J. Snaedal, S. Bjornsson, J. Huttenlocher, A. I. Levey, J. J. Lah, D. Rujescu, H. Hampel, I. Giegling, O. A. Andreassen, K. Engedal, I. Ulstein, S. Djurovic, C. Ibrahim-Verbaas, A. Hofman, M. A. Ikram, C. M. van Duijn, U. Thorsteinsdottir, A. Kong, K. Stefansson, Variant of TREM2 associated with the risk of Alzheimer's disease. *N. Engl. J. Med.* **368**, 107–116 (2013).
21. A. Gal, Y. Li, D. A. Thompson, J. Weir, U. Orth, S. G. Jacobson, E. Apfelstedt-Sylla, D. Vollrath, Mutations in MERTK, the human orthologue of the RCS rat retinal dystrophy gene, cause retinitis pigmentosa. *Nat. Genet.* **26**, 270–271 (2000).
22. G. C. Brown, J. J. Neher, Microglial phagocytosis of live neurons. *Nat. Rev. Neurosci.* **15**, 209–216 (2014).
23. H. H. Klünemann, B. H. Ridha, L. Magy, J. R. Wherrett, D. M. Hemelsoet, R. W. Keen, J. L. De Bleecker, M. N. Rossor, J. Marienhagen, H. E. Klein, L. Peltonen, J. Paloneva, The genetic causes of basal ganglia calcification, dementia, and bone cysts: *DAP12* and *TREM2*. *Neurology* **64**, 1502–1507 (2005).
24. L. Fourgeaud, P. G. Través, Y. Tufail, H. Leal-Bailey, E. D. Lew, P. G. Burrola, P. Callaway, A. Zagórska, C. V. Rothlin, A. Nimmerjahn, G. Lemke, TAM receptors regulate multiple features of microglial physiology. *Nature* **532**, 240–244 (2016).
25. C. Lai, G. Lemke, An extended family of protein-tyrosine kinase genes differentially expressed in the vertebrate nervous system. *Neuron* **6**, 691–704 (1991).
26. J. D. Cahoy, B. Emery, A. Kaushal, L. C. Foo, J. L. Zamanian, K. S. Christopherson, Y. Xing, J. L. Lubischer, P. A. Krieg, S. A. Krupenko, W. J. Thompson, B. A. Barres, A transcriptome database for astrocytes, neurons, and oligodendrocytes: A new resource for understanding brain development and function. *J. Neurosci.* **28**, 264–278 (2008).
27. Y. Zhang, K. Chen, S. A. Sloan, M. L. Bennett, A. R. Scholze, S. O'Keeffe, H. P. Phatnani, P. Guarnieri, C. Caneda, N. Ruderisch, S. Deng, S. A. Liddelow, C. Zhang, R. Daneman, T. Maniatis, B. A. Barres, J. Q. Wu, An RNA-sequencing transcriptome and splicing database of glia, neurons, and vascular cells of the cerebral cortex. *J. Neurosci.* **34**, 11929–11947 (2014).
28. R. A. Hill, E. C. Damisah, F. Chen, A. C. Kwan, J. Grutzendler, Targeted two-photon chemical apoptotic ablation of defined cell types in vivo. *Nat. Commun.* **8**, 15837 (2017).
29. A. Watakabe, M. Ohtsuka, M. Kinoshita, M. Takaji, K. Isa, H. Mizukami, K. Ozawa, T. Isa, T. Yamamori, Comparative analyses of adeno-associated viral vector serotypes 1, 2, 5, 8 and 9 in marmoset, mouse and macaque cerebral cortex. *Neurosci. Res.* **93**, 144–157 (2015).
30. M. Miyanishi, K. Tada, M. Koike, Y. Uchiyama, T. Kitamura, S. Nagata, Identification of Tim4 as a phosphatidylserine receptor. *Nature* **450**, 435–439 (2007).
31. R. Hanayama, M. Tanaka, K. Miwa, A. Shinohara, A. Iwamatsu, S. Nagata, Identification of a factor that links apoptotic cells to phagocytes. *Nature* **417**, 182–187 (2002).
32. M. Nakayama, H. Akiba, K. Takeda, Y. Kojima, M. Hashiguchi, M. Azuma, H. Yagita, K. Okumura, Tim-3 mediates phagocytosis of apoptotic cells and cross-presentation. *Blood* **113**, 3821–3830 (2009).
33. R. S. Scott, E. J. McMahon, S. M. Pop, E. A. Reap, R. Caricchio, P. L. Cohen, H. S. Earp, G. K. Matsushima, Phagocytosis and clearance of apoptotic cells is mediated by MERTK. *Nature* **411**, 207–211 (2001).
34. W.-S. Chung, L. E. Clarke, G. X. Wang, B. K. Stafford, A. Sher, C. Chakraborty, J. Joung, L. C. Foo, A. Thompson, C. Chen, S. J. Smith, B. A. Barres, Astrocytes mediate synapse elimination through MEGF10 and MERTK pathways. *Nature* **504**, 394–400 (2013).
35. M. R. P. Elmore, A. R. Najafi, M. A. Koike, N. N. Dagher, E. E. Spangenberg, R. A. Rice, M. Kitazawa, B. Matusow, H. Nguyen, B. L. West, K. N. Green, Colony-stimulating factor 1 receptor signaling is necessary for microglia viability, unmasking a microglia progenitor cell in the adult brain. *Neuron* **82**, 380–397 (2014).
36. E. Joly, D. Hudrisier, What is trogocytosis and what is its purpose? *Nat. Immunol.* **4**, 815 (2003).
37. A. Peters, T. Kemper, A review of the structural alterations in the cerebral hemispheres of the aging rhesus monkey. *Neurobiol. Aging* **33**, 2357–2372 (2012).
38. D. E. Smith, P. R. Rapp, H. M. McKay, J. A. Roberts, M. H. Tuszynski, Memory impairment in aged primates is associated with focal death of cortical neurons and atrophy of subcortical neurons. *J. Neurosci.* **24**, 4373–4381 (2004).
39. T. R. Hammond, C. Dufort, L. Dissing-Olesen, S. Giera, A. Young, A. Wysoker, A. J. Walker, F. Gergits, M. Segel, J. Nemesh, S. E. Marsh, A. Saunders, E. Macosko, F. Ginhoux, J. Chen, R. J. M. Franklin, X. Piao, S. A. McCarroll, B. Stevens, Single-cell RNA sequencing of microglia throughout the mouse lifespan and in the injured brain reveals complex cell-state changes. *Immunity* **50**, 253–271.e6 (2019).
40. G. Ponath, S. Ramanan, M. Mubarak, W. Housley, S. Lee, F. R. Sahinkaya, A. Vortmeyer, C. S. Raine, D. Pitt, Myelin phagocytosis by astrocytes after myelin damage promotes lesion pathology. *Brain* **140**, 399–413 (2017).
41. T. Magnus, A. Chan, R. A. Linker, K. V. Toyka, R. Gold, Astrocytes are less efficient in the removal of apoptotic lymphocytes than microglia cells: Implications for the role of glial cells in the inflamed central nervous system. *J. Neuropathol. Exp. Neurol.* **61**, 760–766 (2002).
42. D. P. Schafer, E. K. Lehrman, A. G. Kautzman, R. Koyama, A. R. Mardinly, R. Yamasaki, R. M. Ransohoff, M. E. Greenberg, B. A. Barres, B. Stevens, Microglia sculpt postnatal neural circuits in an activity and complement-dependent manner. *Neuron* **74**, 691–705 (2012).
43. V. M. Puñal, C. E. Paisley, F. S. Brecha, M. A. Lee, R. M. Perelli, J. Wang, E. G. O'Koren, C. R. Ackley, D. R. Saban, B. E. Reese, J. N. Kay, Large-scale death of retinal astrocytes during normal development is non-apoptotic and implemented by microglia. *PLOS Biol.* **17**, e3000492 (2019).
44. B. P. Daniels, H. Jujjavarapu, D. M. Durrant, J. L. Williams, R. R. Green, J. P. White, H. M. Lazear, M. Gale Jr., M. S. Diamond, R. S. Klein, Regional astrocyte IFN signaling restricts pathogenesis during neurotropic viral infection. *J. Clin. Invest.* **127**, 843–856 (2017).
45. D. Davalos, J. Grutzendler, G. Yang, J. V. Kim, Y. Zuo, S. Jung, D. R. Littman, M. L. Dustin, W.-B. Gan, ATP mediates rapid microglial response to local brain injury in vivo. *Nat. Neurosci.* **8**, 752–758 (2005).
46. A. Nimmerjahn, F. Kirchhoff, F. Helmchen, Resting microglial cells are highly dynamic surveillants of brain parenchyma in vivo. *Science* **308**, 1314–1318 (2005).
47. O. E. Tasdemir-Yilmaz, M. R. Freeman, Astrocytes engage unique molecular programs to engulf pruned neuronal debris from distinct subsets of neurons. *Genes Dev.* **28**, 20–33 (2014).
48. S. Robel, S. Bardehle, A. Lepier, C. Brakebusch, M. Götz, Genetic deletion of *Cdc42* reveals a crucial role for astrocyte recruitment to the injury site in vitro and in vivo. *J. Neurosci.* **31**, 12471–12482 (2011).
49. Q. Lu, M. Gore, Q. Zhang, T. Camenisch, S. Boast, F. Casagranda, C. Lai, M. K. Skinner, R. Klein, G. K. Matsushima, H. S. Earp, S. P. Goff, G. Lemke, Tyro-3 family receptors are essential regulators of mammalian spermatogenesis. *Nature* **398**, 723–728 (1999).
50. C. Condello, P. Yuan, A. Schain, J. Grutzendler, Microglia constitute a barrier that prevents neurotoxic protofibrillar Aβ42 hotspots around plaques. *Nat. Commun.* **6**, 6176 (2015).
51. F. Chen, B. J. Maher, J. J. LoTurco, *PiggyBac* transposon-mediated cellular transgenesis in mammalian forebrain by in utero electroporation. *Cold Spring Harb. Protoc.* **2014**, 741–749 (2014).
52. A. Nimmerjahn, F. Kirchhoff, J. N. D. Kerr, F. Helmchen, Sulforhodamine 101 as a specific marker of astroglia in the neocortex in vivo. *Nat. Methods* **1**, 31–37 (2004).
53. R. A. Hill, J. Grutzendler, In vivo imaging of oligodendrocytes with sulforhodamine 101. *Nat. Methods* **11**, 1081–1082 (2014).

Acknowledgments

Funding: This work was supported by the following grants from the NIH: R01-NS0889734, RF1-AG058257, and Cure Alzheimer's Fund to J.G.; R00-NS099469 and New Vision Award through the Donors Cure Foundation to R.A.H.; Neurosurgery Research and Education Foundation 14-002715/AANS (NREF) and Swebilius Foundation GS051384 to E.C.D.; and NIH-NIAID R01-AI089824 and NIH-NCI R01-CA212376 to C.V.R. and S.G. C.V.R. is a Howard Hughes Faculty Scholar. **Author contributions:** E.C.D., R.A.H., and J.G. conceived and designed all experiments. E.C.D. and R.A.H. performed all experiments. A.R. contributed to the characterization and quantification of all immunofluorescence experiments. F.C. performed in utero electroporation and obtained some early confocal imaging. C.V.R. and S.G. contributed transgenic mice and provided guidance on experimentation. E.C.D. and J.G. wrote the manuscript. All authors edited the manuscript. J.G. directed the study. **Competing interests:** The authors declare that they have no competing interests. **Data and materials availability:** All data needed to evaluate the conclusions in the paper are present in the paper and/or the Supplementary Materials. Additional data related to this paper may be requested from the authors.

Submitted 22 November 2019
Accepted 12 May 2020
Published 26 June 2020
10.1126/sciadv.aba3239

Citation: E. C. Damisah, R. A. Hill, A. Rai, F. Chen, C. V. Rothlin, S. Ghosh, J. Grutzendler, Astrocytes and microglia play orchestrated roles and respect phagocytic territories during neuronal corpse removal in vivo. *Sci. Adv.* **6**, eaba3239 (2020).